Towards Compact Modeling of Noisy Quantum Computers: A Molecular-Spin-Qubit Case of Study

Towards Compact Modeling of Noisy Quantum Computers: a Molecular-Spin-Qubit Case of Study

MARIO SIMONI, Politecnico di Torino, Department of Electronics and Telecommunications, Italy
GIOVANNI AMEDEO CIRILLO, Politecnico di Torino, Department of Electronics and Telecommunications, Italy
GIOVANNA TURVANI, Politecnico di Torino, Department of Electronics and Telecommunications, Italy
MARIAGRAZIA GRAZIANO, Politecnico di Torino, Department of Applied Science and Technology, Italy
MAURIZIO ZAMBONI, Politecnico di Torino, Department of Electronics and Telecommunications, Italy

Classical simulation of Noisy Intermediate Scale Quantum computers is a crucial task for testing the expected performance of real hardware. The standard approach, based on solving Schrödinger and Lindblad equations, is demanding when scaling the number of qubits in terms of both execution time and memory. In this paper, attempts in defining compact models for the simulation of quantum hardware are proposed, ensuring results close to those obtained with standard formalism. Molecular Nuclear Magnetic Resonance quantum hardware is the target technology, where three non-ideality phenomena — common to other quantum technologies — are taken into account: decoherence, off-resonance qubit evolution and undesired qubit-qubit residual interaction. A model for each non-ideality phenomenon is embedded into a MATLAB simulation infrastructure of noisy quantum computers. The accuracy of the models is tested on a benchmark of quantum circuits, in the expected operating ranges of quantum hardware. The corresponding outcomes are compared with those obtained via numeric integration of the Schrödinger equation and the Qiskit's QASMSimulator. The achieved results give evidence that this work is a step forward towards the definition of compact models able to provide fast results close to those obtained with the traditional physical simulation strategies, thus paving the way for their integration into a classical simulator of quantum computers.

CCS Concepts: • **Hardware** → **Emerging technologies**; *Quantum computation*; **Electronic Design Automation**; *Modeling and parameter extraction.*

Additional Key Words and Phrases: molecular qubits, decoherence, crosstalk, quantum circuits, off-resonance

ACM Reference Format:
Mario Simoni, Giovanni Amedeo Cirillo, Giovanna Turvani, Mariagrazia Graziano, and Maurizio Zamboni. 2021. Towards Compact Modeling of Noisy Quantum Computers: a Molecular-Spin-Qubit Case of Study. *ACM J. Emerg. Technol. Comput. Syst.* 37, 4, Article 111 (August 2021), 25 pages. https://doi.org/10.1145/1122445.1122456

Authors' addresses: Mario Simoni, mario.simoni@polito.it, Politecnico di Torino, Department of Electronics and Telecommunications, C.so Duca degli Abruzzi 24, Torino, Italy, 10129; Giovanni Amedeo Cirillo, Politecnico di Torino, Department of Electronics and Telecommunications, C.so Duca degli Abruzzi 24, Torino, Italy, 10129, giovanni_cirillo@polito.it; Giovanna Turvani, giovanna.turvani@polito.it, Politecnico di Torino, Department of Electronics and Telecommunications, C.so Duca degli Abruzzi 24, Torino, Italy, 10129; Mariagrazia Graziano, mariagrazia.graziano@polito.it, Politecnico di Torino, Department of Applied Science and Technology, C.so Duca degli Abruzzi 24, Torino, Italy, 10129; Maurizio Zamboni, Politecnico di Torino, Department of Electronics and Telecommunications, C.so Duca degli Abruzzi 24, Torino, Italy, 10129, maurizio.zamboni@polito.it.

1 INTRODUCTION

Quantum computing is not just an innovation: it is an actual change of paradigm. Intrinsic properties of quantum mechanics, like superposition, entanglement and interference, permit to quantum computers to be in a superposition of basis states. Careful engineering of the associated probability amplitudes gives rise to interference patterns that can be exploited to solve some arduous tasks with fewer calculations than those expected by classical computers. Moreover, the hardware of quantum computers is represented by quantum systems and, thus, quantum computing is expected to be spontaneously suitable to handle the complexity of quantum physical systems, thus facilitating their emulation, paving the way for the discovery of innovative materials or drugs.

Nowadays, there is still limited availability of many-qubit quantum computers, which are affected by several non-ideality phenomena, such as decoherence and relaxation [28]. Different technologies have been proposed for building a quantum computer based on superconducting devices [20], trapped ions [7], silicon quantum-dots [32] and molecules [13]. Moreover, some devices fabricated by either private companies — *e.g.* superconducting qubits by IBM and trapped ions by Honeywell — or Academia — *e.g.* silicon qubits by QuTech at TU Delft — are already accessible *via* cloud. However, free access is, in general, limited to devices involving few qubits (at most fifteen on IBM hardware) and the available tools do not usually permit to optimise the control and physical parameters affecting the resulting performance. Hence, the development of quantum computing simulators on classical computers could help, on one side, to evaluate the reliability of a quantum algorithm on large amounts of data, with the simulation of circuits involving tens of qubits [35], on the other, it can assist the development of application-driven noise-tolerant quantum algorithms, by taking into account the physical degrees of freedom of quantum hardware. Currently available classical simulators of quantum computers mainly belong to two well-established families:

(1) Fast high-level simulators [1, 16, 18, 35] developed for handling many qubit systems, thus permitting to classically evaluate a quantum algorithm on a large data-set. In order to minimize the simulation latency and to maximise the number of qubits to be simulated, non-ideality phenomena are neglected or described by consolidated mathematical models as Kraus operators formalism for decoherence. [28].
(2) Low-level physical simulators based on the direct integration of Schrödinger and Lindblad equations [17]. Even though this approach is highly accurate at the physical level, it can be extraordinarily memory and CPU-intensive.

The research presented in this work stands between the two families. It is oriented towards the development of a multi-technology simulation infrastructure of noisy quantum computers, based on the definition of *compact models* able to emulate the actual behaviour of real-world quantum hardware, considering the physical parameters affecting the circuit reliability, *e.g.* temperature and duration of quantum gates. Starting from an initial Hamiltonian or phenomenological analysis of the quantum system, the traditional methodologies for the description of the dynamics of qubits are studied and taken into account as a reference for validating and improving the proposed ones, which — even if simplified — never neglect the characteristics of the quantum physical system to be modelled.

The simulation platform is intended to fulfil two objectives. The first one is the execution of the same application-driven quantum circuit on different hardware platforms. The second one is the analysis, for every technology, of the performance dependence on both physical parameters and control degrees of freedom, thus enabling their optimisation according to some fiducial parameters. In conclusion, a common feature of the two goals is the creation of a link between technology and applications. The first attempts of an initial organisation of this simulator were presented in [11], where a `MATLAB`-based simulation infrastructure was introduced, involving three models of molecular quantum computers. The performance of these devices was tested on a benchmark of quantum circuits, by evaluating the effect of

temperature and pulse durations for quantum gates on the fidelity of the quantum states. Moreover, it was ascertained that the Virtual-Z gates [24] always enhance the reliability of the results, thanks to a reduction of the circuit depth.
In this work, non-ideality phenomena shared by different quantum technologies — such as relaxation and decoherence, off-resonance evolution of not-addressed qubits (related to cross-talk) and residual undesired inter-qubit interaction in two-qubit gates — are described by reasonable and CPU-memory friendly models. These are then inserted within the MATLAB-based simulation infrastructure of quantum computing technologies under development. In particular, these models do not resort to the mathematical formalism routinely adopted for the description of these phenomena, which require either the storage of large matrices whose number scales exponentially with the number of qubits, for the evaluation of decoherence, or the calculation of time-domain integrals for evaluating off-resonance evolution. Since homonuclear Nuclear Magnetic Resonance (NMR) quantum computers [33] represent an iconic example of a system affected by the aforementioned phenomena, this paper focuses on this well-known technology. However, pure initial states instead of pseudo-pure states and ideal projective measurements are assumed to decouple the simulation infrastructure from this specific technology and facilitate the extension to non-molecular technologies. The physical parameters of two experimentally-employed molecules are taken into account: two-qubit cytosine [19, 27] and the four-qubit crotonic acid [23, 27, 34]. The developed models have been tested on reversible gates, as CNOT and Toffoli, and on circuits up to four qubits of elementary quantum algorithms, as the Bernstein-Vazirani [5] and Grover's search [14]. In all the analysed cases, the results provided by the new methodology are substantially comparable with those obtained with the standard formalism.
The remaining of this work is organised as follows: Sections 2 and 3 are devolved to a brief presentation of the required mathematical formalism to describe noisy quantum systems and to an overview of NMR quantum computing with the traditional formalism, then Section 4 describes the proposed models for off-resonance evolution and decoherence — with details of the simulation setup in Section 5 — and finally Section 6 collects the results obtained with the standard and the proposed models. The comparison leads to the conclusion that the proposed simulation strategies are reliable and never underestimate the effects of non-ideality phenomena, thus ensuring worst-case scenario results.

2 CLASSICAL MODELLING OF NOISY QUANTUM HARDWARE

2.1 Density matrix formalism

A pure state of a physical system associated with a complex Hilbert space $\mathbb{H}^N$ equipped with an orthonormal basis $|e_i\rangle_{0\leq i<N}$ is described by a state vector $|\psi\rangle = \sum_i c_i |e_i\rangle$, whose evolution is ruled by the Schrödinger equation. However, many quantum physical systems cannot be described by single pure states, on the contrary they are described by **mixed states**. This means that a semi-classical probability distribution of pure states $|\psi_i\rangle$, each of them occurring with a probability p_i, is associated with the quantum state [4, 22, 26]. This formalism is employed for describing quantum systems interacting with the external environment, for instance, through decoherence and relaxation phenomena. In these cases, the most suitable approach is to describe the system by means of the **density matrix**

$$\rho = \sum_i p_i \, |\psi_i\rangle\langle\psi_i| \ . \tag{1}$$

The density matrix of a pure state is $\rho = |\psi\rangle\langle\psi|$. The elements on the main diagonal of ρ are, by definition, the probabilities of finding the system in a basis state. Hence its trace — *i.e.* the sum of the terms on the main diagonal — must be equal to one. The time evolution of a system described by a density matrix ρ is given by the Liouville – von

Neuman equation:

$$i\hbar\frac{\mathrm{d}\rho}{\mathrm{d}t} = [\mathcal{H}(t), \rho]\,, \tag{2}$$

where $\mathcal{H}(t)$ is the Hamiltonian of the system with explicit time dependence and $[x, y] = xy - yx$ is the commutator [28]. As it is routinely done for pure states, also the time evolution of mixed states is customarily represented by employing the unitary time evolution operator $U(t)$:

$$\rho(t) = U(t)\rho(t=0)U(t)^{\dagger}\,, \tag{3}$$

where the time evolution operator $U(t)$ is a formal solution of the Liouville – von Neuman equation

$$U(t) = \mathcal{T}\exp\left\{-\frac{i}{\hbar}\int_0^t \mathcal{H}(\tau)\mathrm{d}\tau\right\}. \tag{4}$$

and $\mathcal{T}$ represents the time-ordered product. If the Hamiltonian can be regarded as not time-dependent, then this operator reduces to

$$U(t) = \exp\left(-i\frac{\mathcal{H}t}{\hbar}\right). \tag{5}$$

The evolution operator is the starting point for the definition of quantum gates and quantum algorithms on physical hardware. Indeed, given a system described by a Hamiltonian $\mathcal{H}_{\mathrm{sys}}(t)$ and a control Hamiltonian $\mathcal{H}_{\mathrm{ctr}}(t;\eta(t))$, a desired unitary transformation U_{alg} can be achieved if there exists a set of control parameters $\eta(t)$ (as the phase and frequency of the radio frequency field) of the total Hamiltonian $\mathcal{H}(t;\eta(t)) = \mathcal{H}_{\mathrm{sys}}(t) + \mathcal{H}_{\mathrm{ctr}}(t;\eta(t))$ such that the time evolution operator [25]

$$U[\eta(t)] = \mathcal{T}\exp\left\{-\frac{i}{\hbar}\int_{t_k}^{t_{k+1}} \mathcal{H}(\tau;\eta(\tau))\mathrm{d}\tau\right\} = e^{-\frac{i}{\hbar}\int_{t_{n-1}}^{t_n}\mathcal{H}(\tau;\eta(t_{n-1}))\mathrm{d}\tau}\cdots e^{-\frac{i}{\hbar}\int_{t_0}^{t_1}\mathcal{H}(\tau;\eta(t_0))\mathrm{d}\tau} \tag{6}$$

is as similar as possible to U_{alg}. In the previous expression $\mathcal{T}$ represents the time-ordered product and the control parameters are taken to be piecewise constant: in each time step $t_k \rightarrow t_{k+1}$ they are chosen such that the corresponding evolution operator implements the desired quantum gate.

2.2 Distance metrics

The evolution of the actual physical device will be in general different from the ideal evolution, because of noise, and, thus, the final outcomes will not be identical. Hence, some metrics are usually introduced to determine how close the actual and ideal outputs are.

Fidelity is a scalar quantity that permits to determine the distance between two quantum states. Here the concept of fidelity as introduced in [28] is adopted. The fidelity between two states represented by density matrices ρ_a and ρ_b is:

$$\mathcal{F}(\rho_a, \rho_b) \triangleq \mathrm{Tr}\left(\sqrt{\rho_a^{1/2}\rho_b\,\rho_a^{1/2}}\right), \tag{7}$$

where Tr is the matrix trace. If one of the two states is described by a state vector $|\psi\rangle$ and the other by a density matrix ρ, the fidelity can be rewritten as

$$\mathcal{F}(|\psi\rangle, \rho) = \sqrt{\langle\psi|\,\rho\,|\psi\rangle}\,. \tag{8}$$

It can be shown that $0 \leq \mathcal{F} \leq 1$ and $\mathcal{F} = 1$ when the two states coincide [28].

The **Kullback-Leibler (KL) divergence** [21, 29] is a measure of the distance between a target discrete probability distribution P and a reference one Q. For instance, the former can come from experimental data and the latter from theoretical deductions. In other words, the main diagonals of two density matrices are sufficient for computing the KL

divergence. This metric has been already employed in [29] for evaluating the reliability of the execution of a circuit on a superconducting quantum computer. For an n-qubit distribution the KL divergence is defined as

$$D_{\mathrm{KL}}(P \parallel Q) \triangleq \sum_{i=0}^{N-1} P(|e_i\rangle) \log_2 \left(\frac{P(|e_i\rangle)}{Q(|e_i\rangle)} \right), \tag{9}$$

where $N = 2^n$ and $|e_i\rangle_{0 \le i < N}$ are the orthonormal eigenstates of the σ_z operator ($|0 \cdots 0\rangle, \cdots, |1 \cdots 1\rangle$). Differently from fidelity, the KL-divergence does not have an upper bound, while the lower one (*i.e.*, $D_{\mathrm{KL}} = 0$) is achieved if and only if the two distributions coincide; therefore, the smaller $D_{\mathrm{KL}}(P \parallel Q)$ is, the closer P and Q are.

3 OVERVIEW OF NUCLEAR MAGNETIC RESONANCE QUANTUM COMPUTING

3.1 Single spin

A nucleus with non-null spin subjected to a static field B_0 is described by the Hamiltonian $\mathcal{H}_0 = -\gamma_n B_0 I_z$ [30], where γ_n is the nuclear gyromagnetic ratio and I_z is the z-component of the spin operator. Since nuclei with spin higher than $1/2$ are known to be characterised by short decoherence times because of quadripolar coupling [30], thus resulting unsuitable for computation, this paper focuses only on spin-$\frac{1}{2}$ nuclei, for which $I_z = \hbar\sigma_z/2$ and similarly for the other components of the spin operator. Therefore, the Hamiltonian becomes $\mathcal{H}_0 = -\hbar\gamma_n B_0 \sigma_z/2$. When $\gamma_n > 0$, which is the common case for the nuclei routinely adopted in NMR based quantum computing experiments, the Hamiltonian reduces to $\mathcal{H}_0 = -\omega_0 I_z$ [30], where $\omega_0 = |\gamma_n| B_0$ is the Larmor frequency.

Identical nuclei in different molecular surroundings experience slightly different local fields B_{loc} [22]. For liquid-state NMR, the dependence of the local field on the applied field is accounted for by the isotropic chemical shielding σ as $B_{\mathrm{loc}} = (1 - \sigma)B_0$ [2]. Hence, the actual Larmor frequency will be correspondingly affected: the shift in the resonance frequency is known as **chemical shift**. Denoting with subscript *ref* the reference compound and with *mol* the molecule under experiment, the chemical shift δ is [2, 30]:

$$\delta \triangleq \frac{\omega_{\mathrm{mol}} - \omega_{\mathrm{ref}}}{\omega_{\mathrm{ref}}} = \frac{\sigma_{\mathrm{ref}} - \sigma_{\mathrm{mol}}}{1 - \sigma_{\mathrm{ref}}} \,. \tag{10}$$

In the remaining of this paper, ω_0 will refer to the *chemically shifted* Larmor frequency

$$\omega_0 \triangleq |\gamma_n|(1 - \sigma_{\mathrm{mol}})B_0 = (1 + \delta)\omega_{\mathrm{ref}} \,. \tag{11}$$

Consequently, identical isotopes in different molecular surroundings are characterised by different resonance frequencies. To control the $\hat{z}$ component of the spin, that is, to change the energy of the system, an interaction that can favour the transitions between levels is needed. Here, the adopted coupling is an alternating magnetic field applied along $-\hat{x}$ axis with angular frequency ω_r, phase ϕ and amplitude $2B_r$. The corresponding Hamiltonian is

$$\mathcal{H}_r = 2\omega_* \cos(\omega_r t - \phi) I_x \,, \tag{12}$$

where $\omega_* = \gamma_n B_r$. Since B_r is usually from five to seven orders of magnitude smaller than B_0, the alternating field can be regarded as a *perturbation* of $\mathcal{H}_0$. The single spin Hamiltonian in the laboratory frame is then $\mathcal{H} = \mathcal{H}_0 + \mathcal{H}_r$.

3.2 Many spins

Nuclear spins in molecules are not isolated from each other and their coupling is described by an interaction Hamiltonian $\mathcal{H}_{\mathrm{int}}$. For diamagnetic liquid state substances, the direct dipole-dipole interaction is usually negligible and $\mathcal{H}_{\mathrm{int}}$ reduces

to the *indirect* spin-spin coupling term only [2, 3, 22], also known as **J-coupling**:

$$\mathcal{H}_{\text{int}} = \frac{2\pi J}{\hbar}\mathbf{I}_a \cdot \mathbf{I}_b\,, \tag{13}$$

where $\mathbf{I}_a = (I_x^{(a)}, I_y^{(a)}, I_z^{(a)})$ is a spin vector operator that acts only on spin a and J is the complete isotropic J-coupling constant, which can be either positive or negative, and it is always measured in Hz. This coupling causes, at first level, the splitting of resonance lines in NMR spectra, known as fine structure. The practical consequence is that some energy transitions among states will be favoured [33] and, so, this mechanism can be exploited to implement two-qubit gates, as discussed in Section 3.4.

3.3 The multi-spin homonuclear Hamiltonian

Every non-trivial quantum algorithm requires at least two coupled qubits. In this case, the overall Hamiltonian, in the laboratory frame, is [26] the sum of an internal contribution

$$\mathcal{H}_{\text{sys}} = -\omega_{0,0}\mathbb{I}\otimes I_z - \omega_{0,1} I_z \otimes \mathbb{I} + \frac{2\pi J_{0,1}}{\hbar}\sum_{k=x,y,z} I_k \otimes I_k\,, \tag{14}$$

where $\mathbb{I}$ is the identity matrix, and a control term $\mathcal{H}_{\text{ctr}} = \mathcal{H}_{r,0} + \mathcal{H}_{r,1}$, where

$$\mathcal{H}_{r,0} = 2\omega_{*,0}\cos\big(\omega_{r,0}t - \phi_0\big)\left(\frac{\gamma_0}{\gamma_0}\mathbb{I}\otimes I_x + \frac{\gamma_1}{\gamma_0} I_x \otimes \mathbb{I}\right) \quad \text{and} \quad \mathcal{H}_{r,1} = 2\omega_{*,1}\cos\big(\omega_{r,1}t - \phi_1\big)\left(\frac{\gamma_0}{\gamma_1}\mathbb{I}\otimes I_x + \frac{\gamma_1}{\gamma_1} I_x \otimes \mathbb{I}\right). \tag{15}$$

In order to remove the explicit time dependence of the Hamiltonian, the system is transformed [30] to two independent rotating frames at frequencies $\omega_{f,0}$ and $\omega_{f,1}$, resorting to the operator $U_F = R_z(\omega_{f,1}t)\otimes R_z(\omega_{f,0}t)$. The rotating frame Hamiltonian $\widetilde{\mathcal{H}}$ can be shown to be [8]

$$\widetilde{\mathcal{H}} = U_F\mathcal{H}U_F^\dagger - i\hbar U_F\frac{\mathrm{d}U_F^\dagger}{\mathrm{d}t} = U_F\left(\mathcal{H}_{\text{sys}} + \mathcal{H}_{r,0} + \mathcal{H}_{r,1}\right)U_F^\dagger - i\hbar U_F\frac{\mathrm{d}U_F^\dagger}{\mathrm{d}t}\,. \tag{16}$$

To understand the approximations introduced by the proposed model, it is mandatory to analyse the different contributions arising from Equation (16), which, thanks to linearity property, can be individually computed. It is straightforward to see that

$$\widetilde{\mathcal{H}}_0 = U_F\mathcal{H}_0U_F^\dagger - i\hbar U_F\frac{\mathrm{d}U_F^\dagger}{\mathrm{d}t} = (\omega_{f,1} - \omega_{0,1})I_z\otimes\mathbb{I} + (\omega_{f,0} - \omega_{0,0})\mathbb{I}\otimes I_z\,. \tag{17}$$

Next, the interaction Hamiltonian in the rotating frame is

$$\widetilde{\mathcal{H}}_{\text{int}} = U_F\mathcal{H}_JU_F^\dagger = \frac{2\pi J_{0,1}}{\hbar}\left\{\cos\left(\Delta\omega_f t\right)\left[I_x\otimes I_x + I_y\otimes I_y\right] - \sin\left(\Delta\omega_f t\right)\left[I_x\otimes I_y - I_y\otimes I_x\right] + I_z\otimes I_z\right\} \tag{18}$$

where $\Delta\omega_f = \omega_{f,1} - \omega_{f,0}$. If the weak coupling limit holds true [26], that is if $\left|\Delta\omega_f\right| \gg |2\pi J|$, then the timescale τ can be chosen such that $\left|\Delta\omega_f\right|\tau \gg 2\pi \gg |2\pi J|\tau$ and the sinusoidal functions of Equation (18) oscillate rapidly and are averaged to vanish. Hence:

$$\widetilde{\mathcal{H}}_{\text{int}} \sim \frac{2\pi J_{0,1}}{\hbar} I_z\otimes I_z\,, \tag{19}$$

Turning finally to the control Hamiltonian:

$$\begin{aligned}\widetilde{\mathcal{H}}_{r,0} = U_F\mathcal{H}_{r,0}U_F^\dagger = \omega_{*,0}\Big\{&\left[\cos\big(2\omega_{r,0}t - \phi_0\big) + \cos(\phi_0)\right]\mathbb{I}\otimes I_x + \left[\sin\big(2\omega_{r,0}t - \phi_0\big) + \sin(\phi_0)\right]\mathbb{I}\otimes I_y + \\ &+ \frac{\gamma_1}{\gamma_0}\left[\cos(\Omega t - \phi_0) + \cos(\Delta\omega_r t + \phi_0)\right] I_x\otimes\mathbb{I} + \frac{\gamma_1}{\gamma_0}\left[\sin(\Omega t - \phi_0) + \sin(\Delta\omega_r t + \phi_0)\right] I_y\otimes\mathbb{I}\Big\},\end{aligned} \tag{20}$$

where $\Delta\omega_r = \omega_{r,1} - \omega_{r,0}$ and $\Omega = \omega_{r,1} + \omega_{r,0}$ and it is assumed that $\omega_{f,i} = \omega_{r,i}$. Since the radio-frequency field is usually operated at resonance, then $\omega_{r,i} \sim \omega_{0,i}$. Homonuclear spins are characterised by similar (but not identical, thanks to chemical shift) resonance frequencies, thus $\Omega \sim 2\omega_{0,0}$. The terms rapidly oscillating with angular frequency Ω, for a time scale τ such that $|\Omega|\tau \gg 2\pi$, can be safely dropped, according to the rotating wave approximation (RWA). Under these assumptions [25]:

$$\widetilde{\mathcal{H}}_{r,0} \sim \omega_{*,0} \left\{ \cos(\phi_0)\mathbb{I} \otimes I_x + \sin(\phi_0)\mathbb{I} \otimes I_y + \frac{\gamma_1}{\gamma_0} \left[\cos(\Delta\omega_r t + \phi_0) I_x \otimes \mathbb{I} + \sin(\Delta\omega_r t + \phi_0) I_y \otimes \mathbb{I} \right] \right\}, \tag{21}$$

In heteronuclear molecules $\Delta\omega_r \sim \Delta\omega_0$ is large and the terms in the square brackets of Equation (21), which make the Hamiltonian time-dependent, can be neglected. However, this is not the case for homonuclear molecules, where the difference in resonance frequencies depends exclusively on the chemical shifts, which are in the order of some parts per million. The terms oscillating at $\Delta\omega_r$ can be dropped in homonuclear molecules if and only if *the pulse width τ is sufficiently long* such that $|\Delta\omega_0\tau| \gg 2\pi$. A pulse that satisfies this requirement is known as soft pulse, in contrast with hard pulses, routinely employed in heteronuclear molecules. The derivation of $\widetilde{\mathcal{H}}_{r,1}$ is akin.
Therefore, if the weak coupling limit assumption, the rotating wave approximation and the soft pulse hypothesis hold true, then the rotating frame Hamiltonian for a homonuclear molecule with n nuclear spins is

$$\widetilde{\mathcal{H}} = \sum_{i=0}^{n-1} (\omega_{f,i} - \omega_{0,i}) I_z^{(i)} + \sum_{i=0}^{n-1} \omega_{*,i} \left[\cos(\phi_i) I_x^{(i)} + \sin(\phi_i) I_y^{(i)} \right] + \sum_{i<k}^{n-1} \frac{2\pi J_{i,k}}{\hbar} I_z^{(i)} I_z^{(k)} . \tag{22}$$

3.4 The NMR quantum computer

It is well-known that one-qubit gates R_x and R_y and the controlled-Z gate (CZ) constitute a universal set of quantum gates [10]. This Section explains how to employ the previously introduced time-independent Hamiltonian to implement quantum gates on homonuclear molecules. The idea is to encode the information on nuclear spins subjected to a static field B_0, to which a resonant radio-frequency field of amplitude B_r is superimposed for a time τ, giving rise to a square pulse.

3.4.1 One-qubit gates. If the hypotheses enumerated at the end of Section 3.3 hold, if the pulse width is such that $|\Delta\omega_0|\tau \gg 2\pi \gg |2\pi J|\tau$, that is, the effect of J-coupling is negligible in the time scale of one-qubit gates, if $\omega_{f,i} = \omega_{r,i}$, and, finally, if the applied RF field is resonant with qubit k ($\omega_{r,k} = \omega_{0,k}$), then the Hamiltonian reduces to $\mathcal{H} \sim \mathcal{H}_{r,k}$ and time evolution operator is:

$$U(\tau) \sim \mathbb{I}^{\otimes(n-1-k)} \otimes \exp\left\{ -i\frac{\theta}{2} [\cos(\phi_k)\sigma_x + \sin(\phi_k)\sigma_y] \right\} \otimes \mathbb{I}^{\otimes k}, \tag{23}$$

which describes a rotation of qubit k of an angle $\theta = \omega_{*,k}\tau$ about the axis $\begin{pmatrix} \cos(\phi_k) & \sin(\phi_k) & 0 \end{pmatrix}$, in the rotating frame. Hence, properly tuning the control parameters τ, ω_* and ϕ, arbitrary rotations about the $\hat{x}$ and $\hat{y}$ axes can be implemented. The Hadamard gate can be decomposed in $\hat{x}$ and $\hat{y}$ rotations as

$$\mathrm{H} \sim -i\mathrm{H} = R_x(\pi) R_y\left(\frac{\pi}{2}\right) \tag{24}$$

where the first equality follows from the mapping between unitary gates and special unitary gates [26]. Finally, a rotation about the $\hat{z}$ axis of an arbitrary angle α can be achieved [26] as

$$R_z(\alpha) = R_x\left(\frac{\pi}{2}\right) R_y(\alpha) R_x\left(-\frac{\pi}{2}\right) \tag{25}$$

or exploiting the **virtual-z method**, introduced in [24] and explained in [11].

3.4.2 Two-qubit gates. Controlled-X (CX) and controlled-Z (CZ) gates can be implemented by exploiting the J-coupling. Assuming for simplicity that there are only two coupled qubits when no RF field is applied, the Hamiltonian becomes $\widetilde{\mathcal{H}} \sim \widetilde{\mathcal{H}}_{\text{int}}$ and the corresponding evolution operator is

$$U_J(t) \triangleq U(t)\Big|_{\text{no RF field}} = \exp\left(-i\frac{\pi J_{0,1}}{2}\sigma_z \otimes \sigma_z t\right) \tag{26}$$

which is here defined as $U_J(t)$ for notation convenience. It can be shown that, when $|q_0\rangle$ is the control qubit and $|q_1\rangle$ is the target qubit, the controlled-Z and controlled-X gates can be implemented as [26, 30, 33]:

The controlled-Z gate:

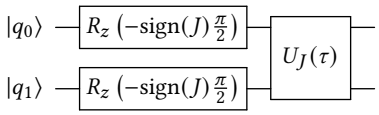

The controlled-X gate:

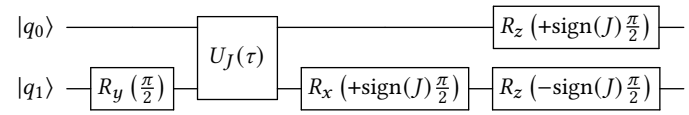

where the operator $U_J(\tau)$ prescribes a free evolution, for a time $\tau = |1/2J|$, under the J-coupling only. Since even if $J < 0$, the time duration τ must be positive to have a physical meaning, some rotations must be modified according to the sign of the coupling constant, to obtain the desired evolution.

3.4.3 Interaction on-demand. In a molecule with several coupled qubits, one-qubit operations can usually be safely executed since their time scale is shorter than $1/J$ and so the effect of J-coupling is negligible, even if particular attention must be paid to long soft pulses. On the other hand, two-qubit operations involve a specific J-coupling: it is mandatory to remove the *other unwanted* J-*couplings* to execute the expected algorithm. This interaction on demand is achieved thanks to a technique known as **refocusing**. The basic principle to remove an unwanted coupling between qubit $|q_k\rangle$ and qubit $|q_m\rangle$ for a time τ is to leave $|q_k\rangle$ to evolve freely between 0 and $\tau/2$ and then reverse its evolution from $\tau/2$ to τ applying a π-pulse on qubit $|q_m\rangle$ at time $t = \tau/2$. A final π-pulse on qubit $|q_m\rangle$ ensures that both qubits return to their initial state. The mathematical foundation of the refocusing technique is that $R_x(-\pi)I_zR_x(+\pi) = -I_z$ from which it follows that in general [33]:

$$[R_x(\pi) \otimes \mathbb{I}]\, U_J\left(\frac{\tau}{2}\right) [R_x(\pi) \otimes \mathbb{I}] = U_J\left(-\frac{\tau}{2}\right) = [\mathbb{I} \otimes R_x(\pi)]\, U_J\left(\frac{\tau}{2}\right) [\mathbb{I} \otimes R_x(\pi)]\ , \tag{27}$$

which means that the application of the π-pulses is equivalent to reversing the direction of time. Hence

$$[R_x(\pi) \otimes \mathbb{I}]\, U_J\left(\frac{\tau}{2}\right) [R_x(\pi) \otimes \mathbb{I}]\, U_J\left(\frac{\tau}{2}\right) = \mathbb{I}\,. \tag{28}$$

Refocusing schemes for multi-qubit systems can be derived from these principles and are discussed in [26, 33]. The most common one is based on Hadamard matrices.

4 MODELING OF NOISY QUANTUM COMPUTERS

4.1 Homonuclear qubit manipulation

The computation of the exact unitary evolution corresponding to the Hamiltonian in Equation (21) requires to carry out a time integration, a computationally expensive operation. On the other hand, the approximated time-independent Hamiltonian of Equation (22) neglects the off-resonance phenomenon. This section presents a model based on the Fourier transform that allows to treat the target qubit according to Equation (22), taking at the same time into account the off-resonance evolution of non-addressed qubits.

According to a practical rule of NMR spectroscopy, longer pulses in the time domain are more selective in the frequency domain since their spectra are narrower; this permits to increase the addressability of single homonuclear qubits. From a mathematical point of view, the effect of soft pulses consists in making the off-resonance term of the Hamiltonian in Equation (21) negligible in the corresponding unitary evolution. This experimental argument can help in the definition of a simplified description of single-qubit gates based on the Fourier analysis. Before going into the details, it could be convenient to understand the expected outcome of the analysis and how this affects the simulation of homonuclear spins. The goal is to compute an effective single-qubit-gate unitary evolution when the l^{th} qubit among n homonuclear qubits is rotated by an amount θ. An equivalent resonant oscillation is assumed to be applied on each qubit and each oscillation, in general, differs from the others in terms of amplitude, so that each qubit is subjected to a different effective rotation angle θ_{eff_k}, which is computed by taking into account the Fourier spectrum of the radiation pulse. The total unitary evolution is

$$U(\tau) = \bigotimes_{k=0}^{n-1} \exp\left\{-i\frac{\theta_{\text{eff}_k}}{2}\left[\cos(\phi_l)\sigma_x + \sin(\phi_l)\sigma_y\right]\right\}, \tag{29}$$

where ϕ_l is the phase of the oscillating signal chosen for rotating the target qubit about a specific axis in the xy-plane and θ_{eff_k} is the effective rotation angle of the k^{th} qubit. In an ideal case, $\theta_{\text{eff}_l} = \theta$ and $\theta_{\text{eff}_k} = 0$ for each qubit k different from the target one.

The Fourier analysis starts from observing that the effect of a magnetic field with amplitude $2B_r$ oscillating on the $\hat{x}$ axis at frequency ω_r on a qubit of gyromagnetic ratio γ_n can be substantially described in terms of an equivalent precession signal

$$\omega_{\text{prec}}(t) = 2m(t)\cos(\omega_r t - \phi), \tag{30}$$

where $m(t) = B_r\gamma_n \cdot s(t) = \omega_* s(t)$ is a modulating signal whose dimension is an angular frequency. If it is assumed that the equivalent precession signal in a frame rotating at frequency ω_r about the $\hat{z}$ axis under the Rotating Wave Approximation corresponds to $m(t)$, the rotation angle of the target qubit is:

$$\theta = \int_{-\infty}^{+\infty} m(t)\mathrm{d}t. \tag{31}$$

If $m(t)$ is assumed to be equal to $\omega_*\mathbf{P}_\tau$, *i.e.* a port signal of duration τ and amplitude ω_*, the angle is exactly equal to

$$\theta = \int_{-\infty}^{+\infty} \omega_*\mathbf{P}_\tau \mathrm{d}t = \omega_* \int_0^\tau \mathrm{d}t = \omega_*\tau, \tag{32}$$

coherently with the formalism reported in Section 3.4.1. The Fourier transform of $m(t)$ is equal to

$$\mathcal{F}\{m(t)\} = M(\Delta\omega) = \int_{-\infty}^{+\infty} m(t)\mathrm{e}^{-\mathrm{i}\Delta\omega t}\mathrm{d}t, \tag{33}$$

where $\Delta\omega = \omega - \omega_r$ is the the independent variable related to the effective angular frequency. Since the model is employed in the rotating frame, the frequency domain of interest is centred at frequency ω_r. It must be observed that the Fourier spectrum has angular dimensions, so that the effective angle of a qubit with resonance frequency ω_k can be computed by evaluating the value of the spectrum at frequency $\omega_k - \omega_r$. For the port signal $m(t) = \omega_*\mathbf{P}_\tau$ the spectrum is

$$\mathcal{F}\{\omega_*\mathbf{P}_\tau\} = \omega_*\tau\,\mathrm{sinc}\left(\frac{\Delta\omega\tau}{2\pi}\right) = \omega_*\tau\frac{\sin\left(\frac{\Delta\omega\tau}{2}\right)}{\frac{\Delta\omega\tau}{2}}, \tag{34}$$

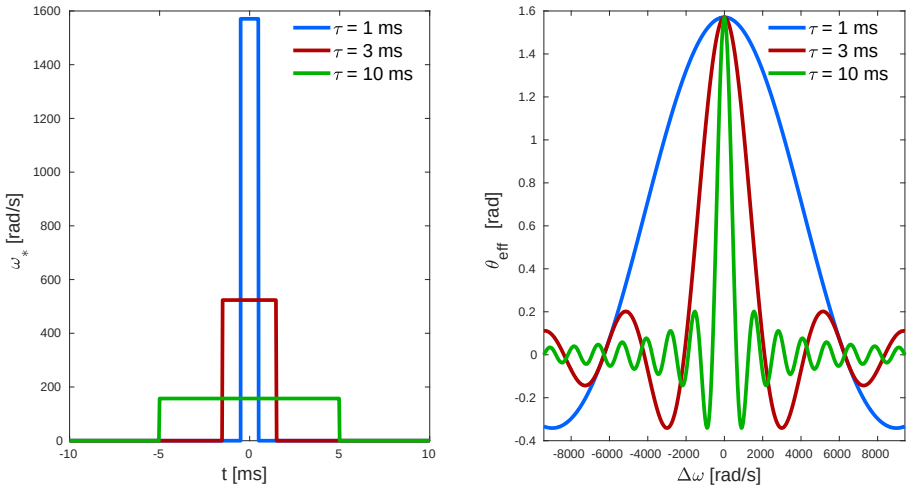

Fig. 1. Effective rotation angles with three different port precession signals.

so that the effective angle of the k^{th} qubit with detuning $\Delta\omega_k = \omega_k - \omega_r$ is computed as

$$\theta_{\text{eff}_k} = \omega_* \tau \, \text{sinc}\left(\frac{\Delta\omega_k \tau}{2\pi}\right). \tag{35}$$

The effective angle of the target qubit, for which $\Delta\omega$ tends to 0, is equal to $\omega_*\tau$, as expected by Equation (32). An important consequence of Equation (34) is that a longer pulse shows a narrower main lobe, thus ensuring a faster achievement of negligible rotation angles for undesired qubits. Figure 1 shows three port precession signals with different τ and same rotation angle $\theta = \frac{\pi}{2}$. The corresponding spectra are all equal to $\frac{\pi}{2}$ when $\Delta\omega \to 0$, but the one corresponding to the pulse with the shortest time duration and highest amplitude (blue in Figure 1) shows the largest lobe. Therefore, the effective rotation angles are in general closer to $\omega_*\tau$, for the same $\Delta\omega_k$.

In conclusion, it is important to highlight that this model is not employable only with port modulating signals. In fact, it can be employed with any $m(t)$ as Gaussian or numerically-optimised pulses, which are usually adopted in NMR spectroscopy.

4.2 Relaxation and Decoherence

Relaxation and decoherence are two dynamic non-ideality phenomena common to all technologies for quantum computing, taking place because of the interactions between qubits, which are not perfectly isolated, and an external environment. The first one is related to the loss of energy of a qubit when it is in its excited state — thus forcing it to reach the ground state after a transient — while the other refers to the dynamic increase of uncertainty about the qubit's phase. These phenomena are recognised as two of the main factors currently limiting the performance of real hardware. After an overview of the traditional mathematical description of relaxation and decoherence, a detailed illustration of the proposed methodology for the modelling of these phenomena is reported.

4.2.1 Traditional formalism. The traditional mathematical description of these phenomena is based on solving the Lindblad equation, an extension of Equation (2) involving a non-unitary contribution to the qubit's evolution [28].

$$\frac{\mathrm{d}\rho}{\mathrm{d}t} = -\frac{i}{\hbar}[\mathcal{H}(t), \rho] + \sum_j [2L_j \rho L_j^\dagger - \{L_j^\dagger L_j, \rho\}], \tag{36}$$

where L_j is a Lindblad operator and $\{x, y\} = xy + yx$ is the anticommutator. In some relevant quantum information cases (*e.g.* the emission of a two-level atom coupled to the vacuum [28]), **Kraus operators** E_k provide evolutions equivalent to those obtained by solving the Lindblad equation. They affect a density matrix ρ according to the following relation:

$$\mathcal{E}(\rho) = \sum_k E_k \rho E_k^\dagger. \tag{37}$$

For an n-qubit system, each operator is a square matrix of size $2^n \times 2^n$ and the total number of involved Kraus operators is at most 2^{2n} [28]. Relaxation of a single qubit can be described in terms of the amplitude damping operators

$$E_0 = \begin{bmatrix} 1 & 0 \\ 0 & \sqrt{1-\gamma} \end{bmatrix} \qquad E_1 = \begin{bmatrix} 0 & \sqrt{\gamma} \\ 0 & 0 \end{bmatrix}, \tag{38}$$

where γ is the probability of changing the qubit state from $|1\rangle\langle 1|$ to $|0\rangle\langle 0|$. E_0 and E_1 change the density matrix according to [28]

$$\mathcal{E}_{\text{ampl. damp.}}(\rho) = \begin{bmatrix} \rho_{0,0} + \gamma\rho_{1,1} & \sqrt{1-\gamma}\rho_{0,1} \\ \sqrt{1-\gamma}\rho_{1,0} & (1-\gamma)\rho_{1,1} \end{bmatrix}. \tag{39}$$

If amplitude damping operators are applied n consecutive times to the qubit, the probability of measuring $|1\rangle\langle 1|$ reduces as $(1-\gamma)^n \rho_{1,1} = \exp(n\log(1-\gamma))\rho_{1,1}$. If $\gamma = \Gamma\Delta t$ — where Γ is the qubit's decay rate — and $n = \frac{t}{\Delta t}$, a continuous-time expression of amplitude damping can be obtained:

$$\lim_{\Delta t \to 0} \exp\Big(\frac{t}{\Delta t}\log(1-\Gamma\Delta t)\Big)\rho_{1,1} \approx \exp\left(-\frac{\Gamma\Delta t}{\Delta t}t\right)\rho_{1,1} = \exp\left(-\frac{t}{T_1}\right)\rho_{1,1}, \tag{40}$$

where $T_1 = \Gamma^{-1}$ is the relaxation time constant. The same exponential scaling takes place in the enhancement of the probability of measuring $|0\rangle\langle 0|$ while the off-diagonal terms show an exponential scaling with time constant $2T_1$.
Decoherence can be described in terms of phase damping operators

$$E_0 = \begin{bmatrix} 1 & 0 \\ 0 & \sqrt{1-\lambda} \end{bmatrix} \qquad E_1 = \begin{bmatrix} 0 & 0 \\ 0 & \sqrt{\lambda} \end{bmatrix}, \tag{41}$$

where λ can be interpreted as the probability that the state of a qubit is randomly perturbed because of distance interactions (*e.g.* electron states with distant electrical charges). The effect of E_0 and E_1 on the density matrix [28] can be written as:

$$\mathcal{E}_{\text{phase damp.}}(\rho) = \begin{bmatrix} \rho_{0,0} & \sqrt{1-\lambda}\rho_{0,1} \\ \sqrt{1-\lambda}\rho_{1,0} & \rho_{1,1} \end{bmatrix}, \tag{42}$$

so the probability terms are not affected by this phenomenon. Similarly to amplitude damping, it is possible to define an exponential scaling of the off-diagonal terms in the continuous time limit:

$$\sqrt{1-\lambda}\rho_{0,1} \xrightarrow{\Delta t \to 0} \exp\left(-\frac{t}{T_2}\right)\rho_{0,1}, \tag{43}$$

where T_2 is the decoeherence time constant. The simultaneous evaluation of the effects of amplitude damping and phase damping on the off-diagonal elements of the density matrix can be quantified in the definition of an effective

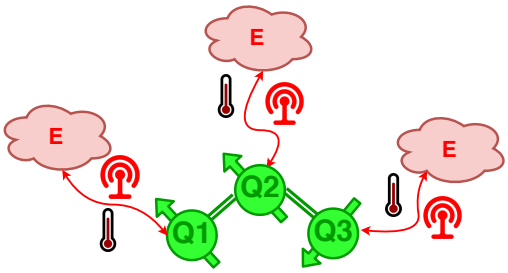

Fig. 2. Equal local baths model, where each qubit interacts thermodynamically or electro-magnetically with a specfic environment.

time constant [1]:

$$T_{2_{\text{eff.}}} \triangleq \left(\frac{1}{2T_1} + \frac{1}{T_2}\right)^{-1}. \tag{44}$$

For what concerns the description of Kraus operators involving multiple qubits, some simplifying assumptions are routinely done. In particular, their construction is usually carried out by combining single-qubit operators with tensor products. This approach is supported in many simulators for quantum computing as the `QasmSimulator` in Qiskit [1]. Even though this formalism can reliably describe the dynamics of an arbitrarily large open quantum system, the classical simulation of the dynamics of a multi-qubit system is computationally demanding. In fact, the exponential scaling of both the dimensions and the total number of Kraus operators requires an exponential increase of the memory, for the simulation of noisy qubits. For this reason, there is an urgent need for an alternative description which can provide a good mimic of the evolution of noisy qubits under relaxation and decoherence, resorting to a reduced amount of hardware resources.

4.2.2 Proposed model. The proposed approach is based on the assumption that the reference physical system employed for describing the dynamics of noisy qubits is based on **equal local baths** [31] (see Figure 2), where each qubit interacts with a separated environment and all the environments are equal, so the decoherence dynamics of each qubit does not depend on the others. In [11] the first attempts for describing the effects of relaxation and decoherence were proposed. The effects of relaxation and decoherence on a single-qubit density matrix in the time domain t can be written as [28]:

$$\begin{bmatrix} (a-a_0)\mathrm{e}^{-\frac{t}{T_1}} + a_0 & b\mathrm{e}^{-\frac{t}{T_2}} \\ b^*\mathrm{e}^{-\frac{t}{T_2}} & (a_0-a)\mathrm{e}^{-\frac{t}{T_1}} + 1 - a_0 \end{bmatrix}, \tag{45}$$

where a and a_0 are the probabilities of measuring the qubit in $|0\rangle\langle 0|$ for $t = 0$ and $t \to \infty$ respectively and T_1 and T_2 are the relaxation and effective decoherence time constants. It can be observed that the effects of relaxation and decoherence are applied locally in density matrices, for this reason, it could be possible to define a simplified strategy for describing these effects without storing all the Kraus operators. Decoherence of an n-qubit system can be modelled with a decoherence matrix D of size $2^n \times 2^n$:

$$\begin{aligned} D &= \bigotimes_{i=n-1}^{0} D_i = D_{n-1} \otimes \cdots \otimes D_0, \\ D_i &\triangleq \begin{bmatrix} 1 & \mathrm{e}^{-\frac{t}{T_{2,i}}} \\ \mathrm{e}^{-\frac{t}{T_{2,i}}} & 1 \end{bmatrix}, \end{aligned} \tag{46}$$

where $\otimes$ refers to the Kronecker product, D_i is the decoherence matrix of the i^{th} qubit among n, with decoherence time constant $T_{2,i}$. The element-by-element product of matrix D with the density matrix is sufficient for evaluating the effect of decoherence. It is possible to ascertain that this is the expected analytical decoherence dynamics of the density matrix in a system with equal local baths [31]. Relaxation was described in [11] by a matrix R, constructed analogously to the n-qubit decoherence matrix:

$$\begin{aligned} R &= \bigotimes_{i=n-1}^{0} R_i = R_{n-1} \otimes \cdots \otimes R_0, \\ R_i &\triangleq \begin{bmatrix} 1 & 1 \\ 1 & \mathrm{e}^{-\frac{t}{T_{1,i}}} \end{bmatrix}, \end{aligned} \tag{47}$$

where R_i is the relaxation matrix of the i^{th} qubit among n, with relaxation time constant $T_{1,i}$. The terms on the main diagonal of R, with the exception of that on the top left associated with the ground basis state $|0\cdots0\rangle\langle0\cdots0|$, are always lower than 1, thus permitting to describe their loss of probability. In order to computationally simplify the description of relaxation, the probability loss was always provided to the ground state, according to the following procedure:

(1) compute the element-by-element product between relaxation and density matrices, so that the generic (i, j) element of the resulting matrix is $\rho_{\text{el-by-el}_{i,j}} = R_{i,j}\rho_{i,j}$;
(2) compute the excited levels loss term as $l = \sum_{i=1}^{2^n-1}(1 - R_{i,i})\rho_{i,i}$ and add it to $\rho_{\text{el-by-el}_{0,0}}$;
(3) assign $\rho_{\text{el-by-el}}$ to ρ.

Even though this procedure describes a dynamics involving a loss of probability of higher-energy states and preserves $\sum_{i=0}^{2^n-1}\rho_{i,i} = 1$, the probability re-distribution between eigenstates is not very accurate, since the ground state and the higher-energy states acquire too much and too little probabilities respectively, if compared to those expected in a real relaxation transient. Moreover, the use of the relaxation matrix R does not equally change the off-diagonal coherence terms of the density matrix, since it tends to change more significantly the terms towards the bottom right corner of ρ. For this reason, a new approach for describing the probability update has been studied and is proposed here. It guarantees, as the one presented in [11], that the trace of the density matrix is always equal to 1. The basic principle is ensuring that a higher probability is provided to states with a larger number of 0 (*i.e.* more qubits in the ground state) and a lower time constant T_1, since they will be subjected to faster transients. Moreover, probability re-distribution is not fixed *a-priori* but is dynamically changed during the simulation, depending on qubits affected by at least one quantum gate.

The first operation of the new approach is evaluating the total lost probability due to relaxation, by computing a **relaxation vector**, instead of a relaxation matrix:

$$\underline{\mathbf{r}} = \bigotimes_{i=n-1}^{0} \begin{bmatrix} 1 \\ \exp\left(-\frac{t}{T_{1_i}}\right) \end{bmatrix} = \left[1, \exp\left(-\frac{t}{T_{1_0}}\right), \cdots, \exp\left(-\sum_{i=0}^{n-1}\frac{t}{T_{1_i}}\right)\right]^{\mathsf{T}} = [r_{0,0}\,,\, r_{1,1}\,,\cdots,\, r_{2^n-1,2^n-1}]^{\mathsf{T}}, \tag{48}$$

so that it is possible to compute the probability lost by each eigenstate as $(1 - r_{k,k})\rho_{k,k}$ and the total lost probability $\mathbb{P}_{\text{lost tot.}} = \sum_{k=0}^{2^n-1}(1 - r_{k,k})\rho_{k,k}$. The relaxation vector affects only the main diagonal of the density matrix and it does not provide any imbalance in the exponential decay of the off-diagonal elements. At this point the new **probability distribution procedure** is applied, which assigns to each eigenstate $|k\rangle$ a probability amount

$$\mathbb{P}_{\text{acquired by }|k\rangle} = \frac{w_{|k\rangle}}{\sum_k w_{|k\rangle}}\mathbb{P}_{\text{lost tot.}}, \tag{49}$$

where $w_{|k\rangle}$ is the weight of each eigenstate and it depends on which qubits have been employed, at the moment of the relaxation evaluation, since the beginning of the quantum circuit simulation. Given the set Q of qubits excited at least once with dimension $\dim(Q)$, $2^{\dim(Q)}$ eigenstates $|k\rangle$ are involved in the relaxation process and each state has a weight equal to:

$$w_{|k\rangle} = \sum_{l \in Q} \frac{1}{T_{1_l}}(1 - b_l), \tag{50}$$

where $b_l = \{0, 1\}$ is the binary value of the qubit l belonging to Q. Therefore, the states with a higher number of $b_l = 0$ and lower relaxation time constants have a higher weight. For example, if some quantum gates have been applied only to two qubits i and j among n, the relaxation process will involve 2^2 eigenstates $|0 \cdots 0\, b_i\, 0 \cdots 0\, b_j\, 0 \cdots 0\rangle$. Each eigenstate $|k\rangle$ among the 2^2 involved has a relaxation weight equal to $w_{|k\rangle} = \frac{1}{T_{1_i}}(1 - b_i) + \frac{1}{T_{1_j}}(1 - b_j)$. Independently from the employed qubits, $|1 \cdots 1\rangle$ has always a weight equal to 0, as it is clear from Equation (50). It is important to further clarify how the weight of a given eigenstate is updated in a simulation, depending on the qubits on which quantum gates have been applied at least once, by considering the case of $|0 \cdots 0\rangle\langle 0 \cdots 0|$. If, at the beginning of a quantum circuit, a quantum gate is applied to the qubit 0, $|0 \cdots 0\rangle$ has a weight equal to $\frac{1}{T_{1_0}}$. Finally, if all qubits have been employed since the beginning of the circuit, its weight is $\sum_{i=0}^{N-1} \frac{1}{T_{1_i}}$.
The evaluation of relaxation can be summarised as follows:

(1) compute the probability lost for each eigenstate $(1 - r_{k,k})\rho_{k,k}$;
(2) compute the total lost probability $\mathbb{P}_{\text{lost tot.}} = \sum_k (1 - r_{k,k})\rho_{k,k}$;
(3) evaluate the eigenstates $|k\rangle$ affected by relaxation;
(4) compute $w_{|k\rangle}$ and consequently $\mathbb{P}_{\text{acquired by } |k\rangle}$;
(5) update the main diagonal of the density matrix according to $\rho_{k,k} = (1 - r_{k,k})\rho_{k,k} + \mathbb{P}_{\text{acquired by } |k\rangle}$.

This simulation strategy permits to significantly reduce the amount of required memory, since a square matrix of size $2^n \times 2^n$ and a vector of length 2^n are sufficient for estimating the dynamics.

5 SIMULATION SETUP

This section describes the simulation setup adopted to validate the proposed models (whose block scheme is reported in Figure 3) and the corresponding assumptions. The same configuration parameters — such as the qubit timescales T_1 and T_2, the duration of quantum gates and the quantum circuits to be tested described in OpenQASM language [12] — are provided to the `MATLAB` simulator, taking into account the discussed models of homonuclear qubits, and to a simulator available in Qiskit framework [1]. The `MATLAB` simulator returns the fidelity and the probability distribution of eigenstates: the former is exploited for comparing the Fourier manipulation model with a numeric Hamiltonian integration, the latter is compared in terms of KL divergence with a corresponding distribution computed with a noise model employable in Qiskit's simulator.

5.1 General assumptions

The proposed simulation infrastructure shall be intended as a general methodology to model the behaviour of quantum hardware affected by non-idealities and the NMR technology is chosen only as an iconic example. Therefore, the infrastructure shall leave aside some experimental peculiarities of NMR hardware.
Firstly, conventional NMR experiments deal with a large ensemble of spins and the corresponding density matrix (ρ_0)

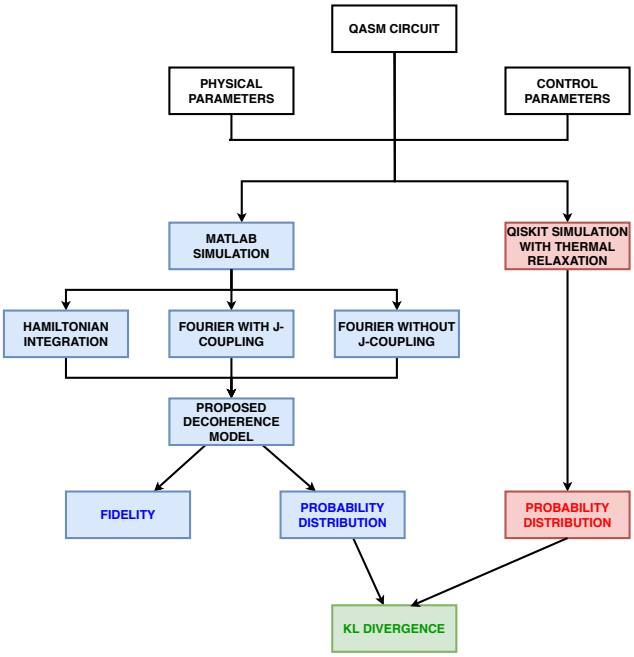

Fig. 3. Block scheme of the simulation procedure.

at thermal equilibrium (high-temperature limit) is a statistical mixture [25, 30]:

$$\rho_0 = \frac{\exp\left(-\frac{\mathcal{H}_{\text{sys}}}{k_{\text{B}}T}\right)}{\text{tr}\left\{\exp\left(-\frac{\mathcal{H}_{\text{sys}}}{k_{\text{B}}T}\right)\right\}} \sim \left(\frac{\mathbb{I}}{2}\right)^{\otimes n} + \Delta\rho\,, \tag{51}$$

where k_{B} is the Boltzmann constant and T is the temperature. The first term is a uniformly mixed ensemble of all possible states, while the second term represents a small deviation. This state is inadequate for computation and there exist several techniques [25] to obtain **pseudopure fiducial initial states** as

$$\rho_0 = \left(\frac{\mathbb{I}}{2}\right)^{\otimes n} + \Delta\rho \longrightarrow \rho_0 = \left(\frac{\mathbb{I}}{2}\right)^{\otimes n} + \alpha\left(|0\rangle\langle 0|\right)^{\otimes n}\,, \tag{52}$$

where α is a small constant. The model discussed in this paper assumes that the initial state is a **pure fiducial initial state**.

Secondly, as mentioned in Section 3.4.3, the implementation of two-qubit quantum gates requires the evolution under J-coupling between a couple of qubits, while the interactions with the other qubits must be switched off by applying the **refocusing techniques**. In order not to overly complicate the model and cause a useless increase of the CPU time required to run the simulation, the refocusing technique is emulated by assuming that the unwanted interactions are turned off.

Thirdly, as known from Equation (11), the computation of the chemically shifted Larmor frequency requires the isotropic chemical shift constant δ and the reference angular frequency ω_{ref}. The chemical shifts come from the experimental values reported in the Spectral Database for Organic Compound SDBS [27], while the reference frequencies are assumed

to be the product of the static field B_0 and the nuclear gyromagnetic ratio γ_n. Hence, the chemical shielding of the reference compound is conventionally assumed to be equal to zero and thus $\omega_0 = (1+\delta)|\gamma_n|B_0$, where $B_0 = 11.74\,\mathrm{T}$ is a reasonable value for NMR instrumentation [26].
Finally, measurement operation is not modelled, *i.e.* when a measurement call is provided to the simulator, it returns the main diagonal of the density matrix corresponding to the qubits' probability distribution.

5.2 Model structure and interface

The proposed model for homonuclear NMR and, in general, for spin-based quantum hardware with qubits characterised by close resonance frequencies is embedded in the simulation infrastructure presented in [11]. Accordingly:

- The quantum algorithm description is read from a `.qasm` file written according to **OpenQASM**, a quantum hardware description language proposed by IBM [12].
- The system is initialised in its pure ground state, corresponding to a density matrix $\rho_{\text{init}} = (|0\rangle\langle 0|)^{\otimes n}$, as previously highlighted.
- Each quantum gate is applied for a time amount τ, thus changing both ρ (physical evolution) and $|\psi_{\text{ideal}}\rangle$ (ideal evolution). In the same time interval, the effects of non-ideality phenomena on the density matrix are evaluated.
- After a measurement operation call, the infrastructure provides in output the ideal outcomes, those obtained via numerical integration, those obtained resorting to the proposed model and the corresponding fidelities.

5.3 Homonuclear model validation

The model introduced in Section 4.1 adopts the **time-independent** Hamiltonian of Equation (22), with the corresponding set of approximations. The weak coupling limit removes the J-coupling interactions along the $\hat{x}$ and $\hat{y}$ axes and makes the interaction Hamiltonian time-independent. The RWA and the use of soft pulses remove the time-dependence from the control Hamiltonian. However, the off-resonance evolution of not-addressed qubits due to the small difference in resonance frequencies is taken into account thanks to the techniques proposed in Section 4.1, without computing any time-domain integral, thus resulting in shorter simulation times. To validate the proposed simulation methodology, the obtained results are compared with the outcomes produced by a **direct numerical integration**, according to Equation (4), of the complete time-dependent rotating-frame Hamiltonian of Equation (16), resorting to `MATLAB`. The latter, as mentioned above, takes into account the J-coupling along the $\hat{x}$ and $\hat{y}$ axes, too. Two and four-qubit quantum circuits are used as benchmarks and the evolution corresponding to each quantum gate is simulated according to both approaches. It has to be remarked that both methods adopt the decoherence model proposed in Section 4.2.2 and resort to the assumptions of Section 5.1.

In the evaluation of the evolution of single-qubit gates under the Fourier model, two approaches are followed:

(1) unitary evolution computed as the exponential of the complete time-independent Hamiltonian of Equation (22), which considers the J-coupling term together with those associated with effective angles;
(2) calculation of unitary evolution as the product of two operators, similarly to a Trotter – Suzuki expansion: one more significantly affecting the evolution on a single-qubit timescale and associated with the effective angles (Equation (29)), the other less significant on the same time interval and related to J-coupling terms only (last term of Equation (22)).

The two-evolution-product approximation is theoretically applicable since the time duration of single-qubit gates is significantly shorter than $\frac{1}{J_{\max}}$, according to Section 5.5. This approach, which does not require the evaluation of a

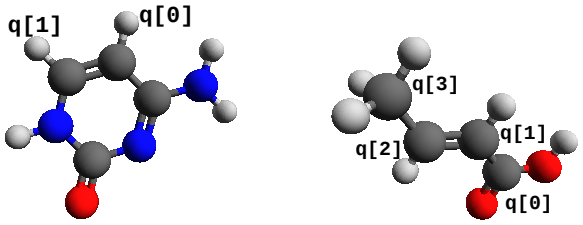

(a) Cytosine. (b) Crotonic acid.

Fig. 4. Employed molecules.

matrix exponential, is here examined to understand if it can provide a further speedup of the simulation, without introducing significant errors.

5.4 Relaxation and decoherence model validation

The proposed methodology for the description of the dynamics of non-ideality relaxation and decoherence phenomena discussed in Section 4.2.2 is compared with a consolidated decoherence model: the thermal relaxation error simulation routine employed by Qiskit's `QasmSimulator`. This error estimate is based on Kraus operators, computed — according to Qiskit [1] documentation — with the time constants T_1 and T_2 of each qubit, quantum gate duration τ, and excited-state thermal population p_1. The time constants are clearly the same employed in the `MATLAB` simulator and p_1 is set to 0, to mimic the relaxation transient described in Section 4.2. Thermal relaxation error is built with quantum gates

$$\begin{aligned} U_2(\phi,\lambda) &= R_z(\phi)R_y\left(\frac{\pi}{2}\right)R_z(\lambda) \\ U_3(\theta,\phi,\lambda) &= R_z(\phi)R_x\left(-\frac{\pi}{2}\right)R_z(\theta)R_x\left(\frac{\pi}{2}\right)R_z(\lambda)\,, \end{aligned} \tag{53}$$

and all R_z gates are virtual, to guarantee that the latency of the quantum circuit is the same in all considered cases. Hence, the duration of a U_2 gate is set equal to that of a $R_{\{x,y\}}\left(\frac{\pi}{2}\right)$ on an NMR quantum computer and that of a U_3 gate is the double of the previous one.

5.5 Physical parameters

The discussed infrastructure is tested by simulating several quantum algorithms on two homonuclear molecules: the cytosine and the crotonic acid (Figure 4). The former is a two-qubit molecule and both qubits are encoded on ^{1}H atoms, whose gyromagnetic ratio is [6]:

$$\gamma_n(^1\mathrm{H}) = 267.519 \times 10^6 \,\mathrm{rad\,s^{-1}\,T^{-1}}\,. \tag{54}$$

The latter is a four-qubit molecule, where the qubits are encoded on ^{13}C atoms, whose gyromagnetic ratio is [6]:

$$\gamma_n(^{13}\mathrm{C}) = 67.283 \times 10^6 \,\mathrm{rad\,s^{-1}\,T^{-1}}\,. \tag{55}$$

The physical parameters of the two molecules are reported in Table 1 and in Table 2.

Table 1. Physical parameters of the crotonic acid: the isotropic chemical shifts [27, 34] are reported on the main diagonal; the J-coupling constants [34] in the off-diagonal terms and the time-constants [23, 34] in the last two rows.

Crotonic Acid				
	q[0]	q[1]	q[2]	q[3]
q[0]	172.35×10^{-6}			
q[1]	72.36 Hz	122.38×10^{-6}		
q[2]	1.18 Hz	69.72 Hz	147.55×10^{-6}	
q[3]	7.04 Hz	1.46 Hz	41.64 Hz	18.08×10^{-6}
T_1	10.20 s	5.60 s	5.30 s	5.10 s
T_2	0.79 s	0.66 s	0.92 s	0.84 s

Table 2. Physical parameters of the cytosine: the isotropic chemical shifts [27] are reported on the main diagonal; the J-coupling constants [19] in the off-diagonal terms and the time-constants [19] in the last two rows.

Cytosine		
	q[0]	q[1]
q[0]	5.970×10^{-6}	
q[1]	7.10 Hz	7.498×10^{-6}
T_1	7.00 s	7.00 s
T_2	1.00 s	1.00 s

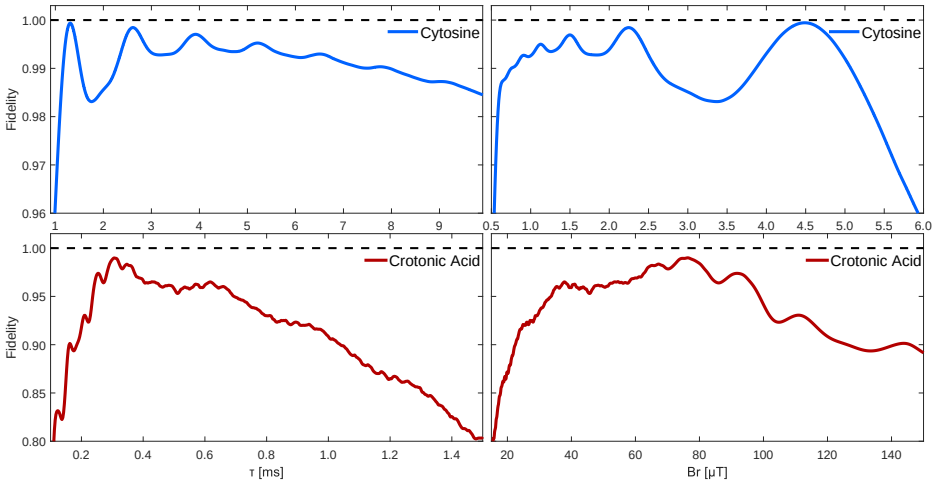

Fig. 5. Fidelity versus pulse width τ and pulse amplitude B_r in a cytosine and in a crotonic acid molecule when a $R_x\left(\frac{\pi}{2}\right)$ rotation is sequentially applied to all qubits.

6 RESULTS

This Section collects the obtained results. Firstly, for each molecule, the RF pulse amplitude is optimised simulating, via direct Hamiltonian integration, the fidelity when a $R_x\left(\frac{\pi}{2}\right)$ rotation is sequentially applied to all qubits, for different values of the pulse width and amplitude. The choice of this kind of benchmark is motivated by the fact that the rotation of $\pi/2$ about $\hat{x}$ axis is a fundamental rotation to implement quantum gates and by the fact that once a qubit is along the $-\hat{y}$ axis, it is sensitive to the unwanted J-coupling evolution which mainly causes an unwanted rotation about $\hat{z}$. Based on the obtained results, the simulation of the execution of several quantum algorithms on both molecules is carried out, comparing the results of the proposed model with those obtained via direct integration and those obtained with Qiskit, according to the approach outlined in Section 5.

6.1 Fidelity optimisation on homonuclear qubits

The behaviour of the fidelity, for different pulse amplitudes and widths, is reported in Figure 5. The range in which τ varies (order of ms) is a clear signature of soft pulses, which must be employed for selective addressing of homonuclear molecules.

6.1.1 Cytosine. The fidelity plot shows a remarkable ringing with local maxima when τ is an integer multiple of $T = 2\pi/|\Delta\omega_0| \sim 1.31\,\text{ms}$. It has to be highlighted that T is the period of the Hamiltonian of Equation (21), where the term in square brackets represents the unwanted effects that a field intended to act on qubit 0 has on qubit 1. Similar considerations apply for the interaction Hamiltonian of Equation (18). Therefore, local maxima occur when the time interval is an integer multiple of the period of the (unwanted) time dependent part of the overall rotating-frame Hamiltonian.
According to Section 3.4, the pulse width shall be such that

$$\frac{2\pi}{|\Delta\omega_0|} \ll \tau \ll \frac{1}{|J|} \longrightarrow 1.31\,\text{ms} \ll \tau \ll 142.86\,\text{ms}\,. \tag{56}$$

Nevertheless, considering Figure 5, it is clear that the upper limit is further reduced by decoherence and relaxation phenomena. Another critical aspect is to take into account the sensitivity of the fidelity F to the fluctuations of the field $(\frac{\partial F}{\partial B_r}\frac{B_r}{F})$ and pulse width $(\frac{\partial F}{\partial \tau}\frac{\tau}{F})$: for instance, the first peak of the fidelity versus time plot is quite narrow and sensible to time variations. The quantum algorithms presented in Section 6.2, are simulated fixing the amplitude of the pulse to a predefined value and varying the pulse width according to the quantum gate that has to be implemented. In this case, the choice can fall on $B_r = 2.27\,\mu\text{T}$, which is a reasonable trade-off between fidelity, its sensitivity and decoherence.

6.1.2 Crotonic acid. The range of pulse width and amplitude values for which the fidelity is acceptable (even if always lower than the cytosine) is limited and significantly smaller compared to cytosine. This is due to the reduced ratio between the largest J-coupling constant and the minimum difference in chemically shifted resonance frequencies:

$$\frac{2\pi}{\left|\Delta\omega_{0,\text{min}}\right|} \ll \tau \ll \frac{1}{|J_{\text{max}}|} \longrightarrow 0.32\,\text{ms} \ll \tau \ll 13.82\,\text{ms}\,. \tag{57}$$

However, according to Figure 5, a trade-off choice is $B_r = 75.45\,\mu\text{T}$. Indeed, being the fidelity relatively low, it is reasonable to choose the maximum value as the working point. The fidelity plot ringing is less evident than for cytosine since there is a $\Delta\omega_0$ for each couple of spins. Nevertheless, it can be argued that local maxima occur in the neighbourhood of integer multiples of $2\pi/\left|\Delta\omega_{0,\text{min}}\right|$, while the fine ringing has a periodicity in the order of $2\pi/\left|\Delta\omega_{0,\text{max}}\right|$.

6.2 Simulation strategies

After defining the optimal pulse for both molecules, the simulation strategies have been characterised with a benchmark of elementary quantum circuits, to be tested on cytosine and crotonic acid molecules. In particular, the simulations are compared in terms of execution time and fidelity of the quantum state to define a trade-off between low latencies and high accuracy of the simplified Fourier models compared to the analytical one based on Hamiltonian integration.
The comparison of simulation times is carried out by taking into account the four-qubit crotonic acid since it permits to better evaluate how latencies, in the proposed strategies, scale with the number of qubits. It can be observed in Table 3 that the simulation times required by the two Fourier methods without virtual-Z gates are very similar, while the Hamiltonian integration requires a CPU time, in general, three orders of magnitude higher than the others, in a better simulation scenario, where $R_z(\theta)$ gates are virtual, thus involving a smaller number of steps. For what concerns fidelity,

Tables 4 and 5 show the results provided by the three strategies with cytosine and crotonic acid respectively. The obtained values are in all cases very close to each other, thus proving that the **simplified Fourier approach** describes the evolution of **hononuclear qubits** under the effect of quantum gates very similarly to a numerical resolution of the Schrödinger equation, requiring significantly **less CPU time**.
The results obtained by treating the evolution due to J-couplings separately from that of single-qubit gate provide higher fidelities of about 1% in many cases. Even though these variations are substantially negligible, the number of simulated qubits is not sufficient for understanding if this approach is too optimistic. Moreover, there is not any significant speedup in the simulation. For these reasons, the two-evolution-product simulation is not employed in the comparison of the decoherence model with respect to Qiskit's thermal relaxation.

Table 3. Fidelities of the two proposed Fourier approaches compared to the distribution obtained with Hamiltonian integration for a crotonic acid molecule. Virtual-Z gates are not employed.

Quantum circuit	Simulation CPU Time Fourier without separated J-coupling No Virtual-Z	Simulation CPU Time Fourier with separated J-coupling No Virtual-Z	Simulation CPU Time Hamiltonian integration Virtual-Z
bern_vaz_101	0.186 s	0.118 s	348.258 s
toffoli_0110	0.451 s	0.521 s	484.498 s
full_adder_0011	1.063 s	1.149 s	982.965 s
swap_03	0.245 s	0.262 s	400.228 s
grover_10_IBMQ	0.224 s	0.263 s	508.787 s
grover_10	0.210 s	0.242 s	502.564 s

Table 4. Comparison of fidelities provided by Fourier approaches and Hamiltonian integration for a cytosine molecule.

Quantum circuit	Fidelity Fourier without separated J-coupling No Virtual-Z	Fidelity Fourier with separated J-coupling No Virtual-Z	Fidelity Hamiltonian integration No Virtual-Z	Fidelity Fourier without separated J-coupling Virtual-Z	Fidelity Fourier with separated J-coupling Virtual-Z	Fidelity Hamiltonian integration Virtual-Z
cnot_01	0.9628	0.9601	0.9597	0.9783	0.9773	0.9771
dcx	0.9243	0.9101	0.9169	0.9560	0.9535	0.9566
iswap_01	0.8828	0.8812	0.8872	0.9269	0.9250	0.9217
dj_balanced	0.9033	0.8892	0.8813	0.9271	0.9251	0.9273
grover_10_IBMQ	0.8712	0.8669	0.8723	0.9269	0.9252	0.9161
grover_10	0.8955	0.8957	0.8959	0.9285	0.9286	0.9202

6.3 Relaxation and decoherence

This section aims at validating the proposed decoherence and relaxation model, as outlined in Section 5.4. In particular, Figure 6 and Figure 7 show the probability distributions for Grover's search and Bernstein-Vazirani's quantum circuits on cytosine and crotonic acid, respectively. These circuits have been chosen because, in both cases, one eigenstate ($|10\rangle$ and $|1101\rangle$ respectively) has a theoretical measurement probability equal to 1. The reported simulations show that the expected outcome is always the most probable: in the cytosine case, the distributions are very close to each other; while, in the crotonic acid case, the peak probability computed according to Qiskit's thermal relaxation model is slightly

Table 5. Comparison of fidelities provided by Fourier approaches and Hamiltonian integration for a crotonic acid molecule.

Quantum circuit	Fidelity Fourier without separated J-coupling No Virtual-Z	Fidelity Fourier with separated J-coupling No Virtual-Z	Fidelity Hamiltonian integration No Virtual-Z	Fidelity Fourier without separated J-coupling Virtual-Z	Fidelity Fourier with separated J-coupling Virtual-Z	Fidelity Hamiltonian integration Virtual-Z
bern_vaz_101	0.7205	0.7201	0.6852	0.9147	0.9128	0.9105
toffoli_0110	0.5589	0.5469	0.5204	0.7692	0.7660	0.7717
full_adder_0011	0.2822	0.2960	0.3357	0.6224	0.6162	0.6190
swap_03	0.8634	0.8359	0.8721	0.9282	0.9262	0.9244
grover_10_IBMQ	0.8260	0.7934	0.8111	0.9649	0.9496	0.9446
grover_10	0.8046	0.8063	0.7993	0.9706	0.9647	0.9575

higher than that resulting from the proposed strategy, irrespectively of the fact that the Fourier model or the direct integration approach is selected. This phenomenon is due to the fact that the proposed re-distribution algorithm keeps more attention on providing the probability lost because of relaxation to all the involved eigenstates. This effect tends to be more evident in circuits involving more qubits. On the other hand, the relaxation mechanism associated with Kraus operators involves few eigenstates in the relaxation dynamics, thus implying a higher probability of the expected outcome. With this in mind, it is possible to understand the results reported in Tables 6 and 7, which show — for each circuit of the employed benchmark — the **most probable eigenstates**, obtained with each simulation approach, and the **KL-divergence** between the probability distributions obtained from Qiskit's thermal relaxation model and those obtained resorting to the proposed one. The most probable eigenstates are the same in all cases. Moreover, the probability distributions corresponding to two-qubit circuits, even if simulated on a crotonic acid molecule and regardless of the circuit depth, are very close to each other, while the KL-divergence is slightly higher in those involving three or four qubits, as the reversible full-adder. However, the highest probability differences and KL-divergences between the reference and the proposed models, which occur for circuits like the reversible full-adder, are not actually critical. In fact, in these cases, the probability value of the expected solution is, with all simulation strategies, sufficiently low (0.5575, 0.3810 and 0.3932 for the full-adder with thermal relaxation, Fourier model and Hamiltonian integration, respectively) for considering unreliable, and thus useless, the execution of those circuits on the target molecules. Moreover, the maximum probabilities obtained with the proposed model are always lower than those based on thermal relaxation, thus ensuring that the proposed methodology does not underestimate the qubits' non-idealities.

In conclusion, the proposed compact model not involving 2^n Kraus operators does **not underestimate** the effects of decoherence compared to a standard representation. Moreover, it tends to spread more significantly the probability lost for relaxation when considering quantum circuits with more qubits. On the contrary, the circuit depth does not significantly affect the variation of the probability distribution compared to the standard model.

7 CONCLUSIONS

Starting from the analysis of the qubits physical systems, in terms of Hamiltonian characterisation and experimental qubit dynamics, some innovative strategies for describing the effects of non-resonant excitations on homonuclear molecular qubits and decoherence have been presented. With this work the **reliability** of the proposed approach for **describing noisy qubits** has been demonstrated, by comparing the results provided by the implemented models with those obtained with numerical solutions of the Schrödinger equation and with existing noise models in Qiskit's

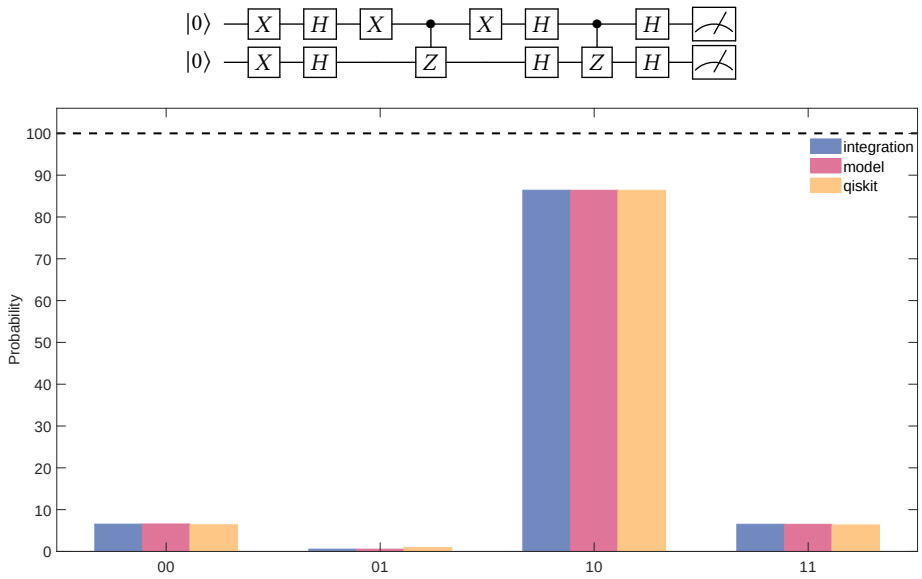

Fig. 6. Probability distribution resulting from the simulation of the execution of Grover's quantum algorithm (binary solution equal to 10) on a cytosine molecule, adopting the direct integration, the proposed model and Qiskit `QasmSimulator`.

Table 6. Comparison of the most probable outcomes on a cytosine quantum computer, according to the thermal relaxation model of Qiskit and two simulation strategies based on the proposed relaxation model. Virtual-Z gates are assumed to be employed.

Quantum Circuit	Qiskit thermal relaxation most probable eigenstate, prob.	Fourier with J-coupling most probable eigenstate KL-Divergence	Hamiltonian integration most probable eigenstate KL-Divergence
cnot_01	$\|11\rangle$, $\mathbb{P} = 0.9541$	$\|11\rangle$, $\mathbb{P} = 0.9550$ KLD = 0.010727	$\|11\rangle$, $\mathbb{P} = 0.9556$ KLD = 0.008759
dcx_01	$\|10\rangle$, $\mathbb{P} = 0.9117$	$\|10\rangle$, $\mathbb{P} = 0.9120$ KLD = 0.001612	$\|10\rangle$, $\mathbb{P} = 0.9100$ KLD = 0.002051
iswap_01	$\|10\rangle$, $\mathbb{P} = 0.8641$	$\|10\rangle$, $\mathbb{P} = 0.8557$ KLD = 0.000514	$\|10\rangle$, $\mathbb{P} = 0.8558$ KLD = 0.000508
dj_balanced	$\|01\rangle$, $\mathbb{P} = 0.8641$	$\|01\rangle$, $\mathbb{P} = 0.8621$ KLD = 0.001697	$\|01\rangle$, $\mathbb{P} = 0.8616$ KLD = 0.001729
grover_10_IBMQ	$\|10\rangle$, $\mathbb{P} = 0.8640$	$\|10\rangle$, $\mathbb{P} = 0.8556$ KLD = 0.000498	$\|10\rangle$, $\mathbb{P} = 0.8567$ KLD = 0.000332
grover_10	$\|10\rangle$, $\mathbb{P} = 0.8639$	$\|10\rangle$, $\mathbb{P} = 0.8639$ KLD = 0.001531	$\|10\rangle$, $\mathbb{P} = 0.8640$ KLD = 0.001656

`QasmSimulator`.

Even though this work does not propose a definitive model for common non-ideality phenomena of quantum computing technologies, the obtained results are encouraging for the accurate simulation of noisy quantum circuits in the future. In fact, it is possible to reduce the required amount of memory for classically describing the evolution of a qubit system under the effect of quantum gates and non-ideality phenomena. Furthermore, the results highlight that reliable qubit dynamics can be achieved without solving any time integral, thus significantly reducing the simulation latency. These

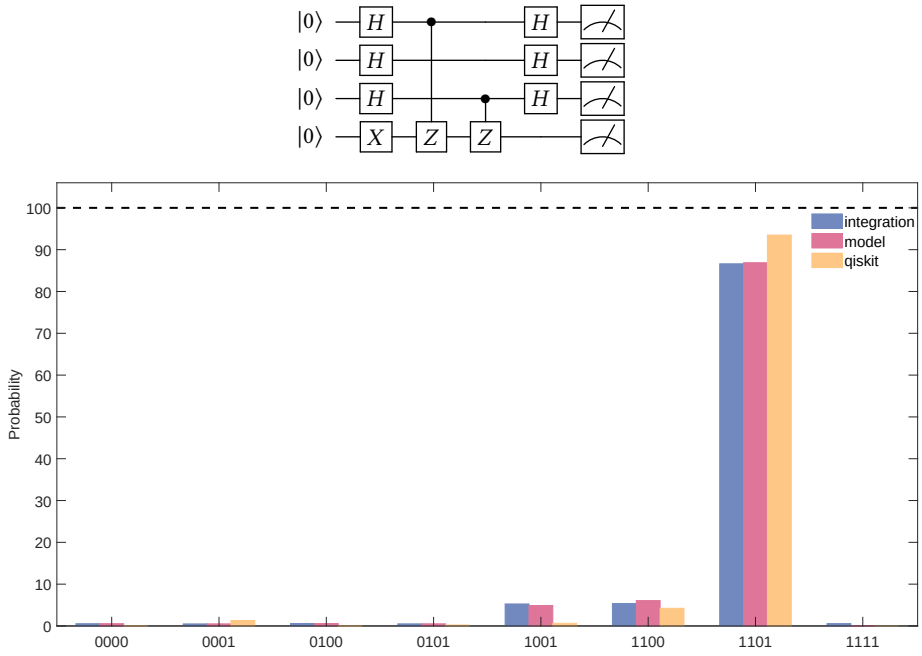

Fig. 7. Probability distribution resulting from the simulation of the quantum circuit of Bernstein-Vazirani's algorithm (binary string to be found equal to 101) on a crotonic acid molecule, adopting the direct integration, the proposed model and Qiskit's `QasmSimulator`. Only the eigenstates with non-null probabilities are reported.

Table 7. Comparison of the most probable outcomes on a crotonic acid quantum computer, according to the thermal relaxation model of Qiskit and two simulation strategies based on the proposed relaxation model. Virtual-Z gates are assumed to be employed.

Quantum Circuit	Qiskit thermal relaxation most probable eigenstate, prob.	Fourier with J-coupling most probable eigenstate KL-Divergence	Hamiltonian integration most probable eigenstate KL-Divergence
bernstein_vazirani_101	$\|1101\rangle$, $\mathbb{P} = 0.9349$	$\|1101\rangle$, $\mathbb{P} = 0.8688$ KLD = 0.071052	$\|1101\rangle$, $\mathbb{P} = 0.8662$ KLD = 0.082697
toffoli_0110	$\|1110\rangle$, $\mathbb{P} = 0.7176$	$\|1110\rangle$, $\mathbb{P} = 0.6282$ KLD = 0.277338	$\|1110\rangle$, $\mathbb{P} = 0.6384$ KLD = 0.253923
full_adder_0011	$\|1001\rangle$, $\mathbb{P} = 0.5575$	$\|1001\rangle$, $\mathbb{P} = 0.3810$ KLD = 0.584241	$\|1001\rangle$, $\mathbb{P} = 0.3932$ KLD = 0.567896
swap_03	$\|1000\rangle$, $\mathbb{P} = 0.8645$	$\|1000\rangle$, $\mathbb{P} = 0.8582$ KLD = 0.005852	$\|1000\rangle$, $\mathbb{P} = 0.8591$ KLD = 0.005729
grover_10_IBMQ	$\|0010\rangle$, $\mathbb{P} = 0.9797$	$\|0010\rangle$, $\mathbb{P} = 0.9337$ KLD = 0.040235	$\|0010\rangle$, $\mathbb{P} = 0.9296$ KLD = 0.049765
grover_10	$\|0010\rangle$, $\mathbb{P} = 0.9796$	$\|0010\rangle$, $\mathbb{P} = 0.9614$ KLD = 0.010340	$\|0010\rangle$, $\mathbb{P} = 0.9464$ KLD = 0.031118

features are highly desirable for developing a classical simulation infrastructure of quantum computing technologies, whose response to quantum gates can be evaluated by taking into account all their main properties and ensuring a good mimic of their expected experimental behaviour. The development of an appropriate simulation infrastructure

will eventually be an essential tool for optimising the execution of quantum circuits on noisy quantum computers, by accurately choosing the qubits' physical and control parameters, such as the duration of $R_x\left(\frac{\pi}{2}\right)$ pulses for maximising the state fidelity. A final simulator undoubtedly requires more research; some of the future steps required to approach this goal, in both hardware modelling and software development domains, are reported in the following.

The infrastructure is going to evaluate the behaviour of different quantum computing technologies, and non-molecular devices are going to be examined. The definition of compact models for new technologies will benefit from those already defined for molecules, inheriting and arranging some features. For example, the decoherence model is not specifically thought for NMR qubits. Conversely, it can be adapted to other devices and to relaxation dynamics where the steady-state is different from $|0\cdots0\rangle\langle0\cdots0|$, by modifying the weights of the re-distribution algorithm. Solid-state devices, such as silicon [32] or nitrogen-vacancy (NV) centers in diamond [9], could be the first ones to be investigated since they encode quantum information onto spins, and so the inheritance of molecular qubit models is potentially easier. Moreover, the effects of single-qubit gates on homonuclear qubits can be generalised to the description of the effects of electromagnetic radiations, *e.g.* due to crosstalk phenomena, on every technology based on qubits characterised by resonance frequencies close to each other.

The simulator will have to follow the expected scaling of the number of qubits in the coming years so that users will always be able to evaluate the performance of their contemporary devices. In this context, smart strategies for the storage of the density matrix shall be found. Indeed, the amount of memory that has to be allocated for simulation scales exponentially with the number of qubits since the standard approach requires storing 2^{2n} complex numbers for n noisy qubits. This significant amount of memory could be reduced by observing that the density matrix often shows repeated identical numbers in some practical quantum algorithms. Therefore, alternative data structures, which store the recurring values of the density matrix only once, will be investigated to enable fast and reliable simulation of tens or hundreds of noisy qubits in the future. A simulation approach based on decision diagrams [15] could be a good starting point for achieving this goal.

Although there are some improvable features, this work is hoped to be a starting point for an accurate infrastructure for classical simulations of noisy quantum computers, which can be successfully employed by circuit designers, with the consciousness that the provided results are very close to those expected in an experimental setup.

REFERENCES

[1] Héctor Abraham, AduOffei, Ismail Yunus Akhalwaya, Gadi Aleksandrowicz, Thomas Alexander, Gadi Alexandrowics, Eli Arbel, Abraham Asfaw, et al. 2019. Qiskit: An Open-source Framework for Quantum Computing. https://doi.org/10.5281/zenodo.2562110

[2] Peter Atkins and Julio de Paula. 2010. *Physical Chemistry* (9 ed.). W H Freeman and Co, New York City, New York.

[3] Jochen Autschbach and Boris Le Guennic. 2007. Analyzing and Interpreting NMR Spin Spin Coupling Constants Using Molecular Orbital Calculations. *Journal of Chemical Education* 84, 1 (2007), 156. https://doi.org/10.1021/ed084p156

[4] Roger Balian. 2007. *From Microphysics to Macrophysics: Methods and Applications of Statistical Physics* (1st ed.). Springer, New York.

[5] Ethan Bernstein and Umesh Vazirani. 1997. Quantum Complexity Theory. *SIAM J. Comput.* 26, 5 (1997), 1411–1473. https://doi.org/10.1137/S0097539796300921

[6] BRUKER Biospin. 2020. NMR Periodic Table. [Online at http://triton.iqfr.csic.es/guide/eNMR/chem/NMRnuclei.html,; accessed 21-November-2020].

[7] Colin D Bruzewicz, John Chiaverini, Robert McConnell, and Jeremy M Sage. 2019. Trapped-ion quantum computing: Progress and challenges. *Applied Physics Reviews* 6, 2 (2019), 021314. https://doi.org/10.1063/1.5088164

[8] John Cavanagh, Wayne J. Fairbrother, Arthur G. Palmer III, Nicholas J. Skelton, and Mark Rance. 2007. *Protein NMR Spectroscopy, Second Edition: Principles and Practice* (2 ed.). Elsevier Academic Press, London, UK.

[9] Lilian Childress and Ronald Hanson. 2013. Diamond NV centers for quantum computing and quantum networks. *MRS Bulletin* 38, 2 (2013), 134–138. https://doi.org/10.1557/mrs.2013.20

[10] G. A. Cirillo, G. Turvani, and M. Graziano. 2019. A Quantum Computation Model for Molecular Nanomagnets. *IEEE Transactions on Nanotechnology* 18 (2019), 1027–1039. https://doi.org/10.1109/TNANO.2019.2939910

[11] G. A. Cirillo, G. Turvani, M. Simoni, and M. Graziano. 2020. Advances in Molecular Quantum Computing: from Technological Modeling to Circuit Design. In *2020 IEEE Computer Society Annual Symposium on VLSI (ISVLSI)*. IEEE, 132–137. https://doi.org/10.1109/ISVLSI49217.2020.00033

[12] Andrew W. Cross, Lev S. Bishop, John A. Smolin, and Jay M. Gambetta. 2017. Open Quantum Assembly Language. arXiv:arXiv:1707.03429v2 https://arxiv.org/abs/1707.03429 Arxiv repository: arXiv:1707.03429.

[13] Alejandro Gaita-Ariño, Fernando Luis, Stephen Hill, and Eugenio Coronado. 2019. Molecular spins for quantum computation. *Nature chemistry* 11, 4 (2019), 301–309. https://doi.org/10.1038/s41557-019-0232-y

[14] Lov K Grover. 1996. A fast quantum mechanical algorithm for database search. In *Proceedings of the twenty-eighth annual ACM symposium on Theory of computing*. Association for Computing Machinery, New York, NY, USA, 212–219. https://doi.org/10.1145/237814.237866

[15] Thomas Grurl, Jürgen Fuß, and Robert Wille. 2020. Considering decoherence errors in the simulation of quantum circuits using decision diagrams. In *Proceedings of the 39th International Conference on Computer-Aided Design*. Association for Computing Machinery, New York, NY, USA, 1–7. https://doi.org/10.1145/3400302.3415622

[16] Gian Giacomo Guerreschi, Justin Hogaboam, Fabio Baruffa, and Nicolas P D Sawaya. 2020. Intel Quantum Simulator: a cloud-ready high-performance simulator of quantum circuits. *Quantum Science and Technology* 5, 3 (5 2020), 034007. https://doi.org/10.1088/2058-9565/ab8505

[17] J Robert Johansson, Paul D Nation, and Franco Nori. 2012. QuTiP: An open-source Python framework for the dynamics of open quantum systems. *Computer Physics Communications* 183, 8 (2012), 1760–1772. https://doi.org/10.1016/j.cpc.2012.02.021

[18] Nader Khammassi, Imran Ashraf, Xiang Fu, Carmen G Almudever, and Koen Bertels. 2017. QX: A high-performance quantum computer simulation platform. In *Design, Automation & Test in Europe Conference & Exhibition (DATE), 2017*. IEEE, 464–469. https://doi.org/10.23919/DATE.2017.7927034

[19] Yasushi Kondo, Mikio Nakahara, Kazuya Hata, and Shogo Tanimura. 2005. Hamiltonian of Homonucleus Molecules for NMR Quantum Computing. arXiv:arXiv:quant-ph/0503067

[20] Philip Krantz, Morten Kjaergaard, Fei Yan, Terry P Orlando, Simon Gustavsson, and William D Oliver. 2019. A quantum engineer's guide to superconducting qubits. *Applied Physics Reviews* 6, 2 (2019), 021318. https://doi.org/10.1063/1.5089550

[21] S. Kullback and R. A. Leibler. 1951. On Information and Sufficiency. *Ann. Math. Statist.* 22, 1 (03 1951), 79–86. https://doi.org/10.1214/aoms/1177729694

[22] Malcolm Levitt. 2008. *Spin dynamics : basics of nuclear magnetic resonance*. John Wiley & Sons, Ltd, Chichester, England Hoboken, NJ.

[23] Keren Li, Youning Li, Muxin Han, Sirui Luand Jie Zhou, Dong Ruan, Guilu Long, Yidun Wa, Dawei Lu, Bei Zeng, and Raymond Laflamme. 2019. Quantum spacetime on a quantum simulator. *Communications Physics* 2, 1 (12 2019), 122–128. https://doi.org/10.1038/s42005-019-0218-5

[24] David C. McKay, Christopher J. Wood, Sarah Sheldon, Jerry M. Chow, and Jay M. Gambetta. 2017. Efficient Z gates for quantum computing. *Phys. Rev. A* 96, 2 (8 2017), 022330. https://doi.org/10.1103/PhysRevA.96.022330

[25] Mikio Nakahara, Shigeru Kanemitsu, Martti Salomaa, and Shin Takagi. 2006. *Physical realizations of quantum computing : are the DiVincenzo criteria fulfilled in 2004?* (1 ed.). World Scientific, Singapore Hackensack, N.J.

[26] Mikio Nakahara and Tetsuo Ohmi. 2008. *Quantum Computing From Linear Algebra to Physical Realizations* (1 ed.). CRC Press, Boca Raton, Florida.

[27] National Institute of Advanced Industrial Science and Technology. 2020. Spectral Database for Organic Compounds. [Online at https://sdbs.db.aist.go.jp,; accessed 17-November-2020].

[28] Michael A. Nielsen and Isaac L. Chuang. 2010. *Quantum Computation and Quantum Information* (10th aniversary ed.). Cambridge University Press, Cambridge.

[29] Shin Nishio, Yulu Pan, Takahiko Satoh, Hideharu Amano, and Rodney Van Meter. 2020. Extracting Success from IBM's 20-Qubit Machines Using Error-Aware Compilation. *ACM Journal on Emerging Technologies in Computing Systems (JETC)* 16, 3 (2020), 1–25. https://doi.org/10.1145/3386162

[30] Ivan S. Oliveira, Tito J. Bonagamba, Roberto S. Sarthour, Jair C.C. Freitas, and Eduardo R. deAzevedo. 2007. *NMR Quantum Information Processing* (1 ed.). Elsevier, Oxford, UK.

[31] G Massimo Palma, Kalle-Antti Suominen, and Artur Ekert. 1996. Quantum computers and dissipation. *Proceedings of the Royal Society of London. Series A: Mathematical, Physical and Engineering Sciences* 452, 1946 (1996), 567–584. https://doi.org/10.1098/rspa.1996.0029

[32] L Petit, HGJ Eenink, M Russ, WIL Lawrie, NW Hendrickx, SGJ Philips, JS Clarke, LMK Vandersypen, and M Veldhorst. 2020. Universal quantum logic in hot silicon qubits. *Nature* 580, 7803 (2020), 355–359. https://doi.org/10.4121/uuid:22653416-85b0-4d7d-ad48-65967f9ea7ad

[33] Lieven MK Vandersypen and Isaac L Chuang. 2005. NMR techniques for quantum control and computation. *Reviews of modern physics* 76, 4 (2005), 1037. https://doi.org/10.1103/RevModPhys.76.1037

[34] Jingwei Wen, Xiangyu Kong, Shijie Wei, Bixue Wang, Tao Xin, and Guilu Long. 2019. Experimental realization of quantum algorithms for a linear system inspired by adiabatic quantum computing. *Phys. Rev. A* 99, 1 (Jan 2019), 012320. https://doi.org/10.1103/PhysRevA.99.012320

[35] Alwin Zulehner and Robert Wille. 2019. Advanced Simulation of Quantum Computations. *Trans. on CAD of Integrated Circuits and Systems* 38, 5 (2019), 848–859. https://doi.org/10.1109/TCAD.2018.2834427